

promoting access to White Rose research papers



Universities of Leeds, Sheffield and York
<http://eprints.whiterose.ac.uk/>

This is the author's post-print version of an article published in the **Journal of Computational Physics**

White Rose Research Online URL for this paper:

<http://eprints.whiterose.ac.uk/id/eprint/76342>

Published article:

Cooper, JD, Valavanis, A, Ikonic, Z, Harrison, P and Cunningham, JE (2013) *Stable perfectly-matched-layer boundary conditions for finite-difference time-domain simulation of acoustic waves in piezoelectric crystals*. *Journal of Computational Physics*, 253. 239 - 246. ISSN 0021-9991

<http://dx.doi.org/10.1016/j.jcp.2013.07.019>

Stable perfectly-matched-layer boundary conditions for finite-difference time-domain simulation of acoustic waves in piezoelectric crystals

J.D. Cooper, A. Valavanis, Z. Ikonić, P. Harrison, J.E. Cunningham

Institute of Microwaves and Photonics, School of Electronic and Electrical Engineering, University of Leeds, Leeds, LS2 9JT, United Kingdom

Abstract

Perfectly matched layer (PML) boundary conditions are derived for finite-difference time-domain analysis of acoustic waves within piezoelectric crystals. The robustness and effectiveness of the derived boundary conditions are demonstrated by simulating acoustic wave propagation in the bismuth germanate material system—a system in which simple absorbing boundary conditions cause instabilities. An investigation into the stability and effectiveness of the PML is then presented in terms of the PML thickness and absorption profile. A range of optimised absorption profiles were determined by finding the maximum permissible absorption within the stability limit of the system. In the optimised case, the form of the absorption profile had little influence on the effectiveness of the PML. However, in the unoptimised case the linearly increasing absorption profile was found to be the most effective.

Keywords: Finite-difference time-domain, Acoustic wave, Perfectly matched layer, Piezoelectric crystal

1. Introduction

The finite-difference time-domain (FDTD) method, introduced by Yee [1] in 1966 for simulating Maxwell's equations, was first applied to the acoustic wave equations of motion in piezoelectric crystals by Smith *et al.* in 2002 [2]. Since the solutions of both these systems involve propagating waves, the method of truncating an otherwise infinite

Email address: e106jdc@leeds.ac.uk (J.D. Cooper)
Preprint submitted to Journal of Computational Physics

simulation domain around some region of interest (ROI) is critical in stopping reflections off these artificial boundaries interfering with the physics being investigated. In 2006, Chagla *et al.* [3] added absorbing boundary conditions to the acoustic wave problem by adding an absorbing layer with a quadratically increasing damping coefficient to dissipate the energy from any oscillations which reach the boundaries. Although this method worked well in some cases, Chagla *et al.* showed that it does not remain stable for all material systems.

Since it was first introduced by Berenger in 1994 [4], the perfectly matched layer (PML) has been used extensively in FDTD simulations of electromagnetic waves. It may be viewed as an analytic continuation of spatial variables onto the complex plane such that any oscillating solution that enters the PML will be transformed into an oscillating component with an exponentially decaying envelope [5]. Despite the ongoing interest in development of the PML [6, 7, 8, 9] in electromagnetic simulations as well as its application in both elastodynamics [10] and fluid dynamics [11], the PML has not been applied to the simulation of acoustic waves in piezoelectric crystals.

In this work, we derive PML boundary conditions for the acoustic wave equations of motion within a piezoelectric crystal by applying a complex coordinate stretching of spatial variables in the frequency domain. The boundary conditions are then transformed back to the time domain and discretised using the same interlaced mesh used by Smith *et al.* such that both the ROI and PMLs may be solved using the same FDTD algorithm, thereby avoiding any increase in computational complexity in the simulation.

The robustness and effectiveness of our PML implementation is demonstrated in the following section, and is shown to be stable for a bismuth germanate material system in which absorbing boundary conditions fail [3]. This is followed by a discussion of the stability criteria for the discretised PML and a quantitative analysis of their effectiveness with respect to their operating parameters as well as optimisation of those parameters.

2. Derivation of PML boundaries for the acoustic wave equations of motion

The equation of motion for an acoustic wave in a piezoelectric crystal is

$$\rho \ddot{u}_i = \frac{\partial \sigma_{ij}}{\partial x_j} \quad \text{for } i, j = 1, 2, 3, \quad (1)$$

where \mathbf{u} is the displacement of a particle in three orthogonal directions x_1 , x_2 and x_3 , and

$$\sigma_i = C_{ij}\epsilon_j + e_{ik}^T \frac{\partial \phi}{\partial x_k} \quad \text{for } i, j = 1, 2, \dots, 6; k = 1, 2, 3, \quad (2)$$

is Hooke's law for piezoelectric crystals, where σ is the stress, C is the elastic constant tensor, e^T is the transpose of the piezoelectric constant tensor, ϕ is the induced piezoelectric potential inside the crystal structure and ϵ is the strain inside the crystal which is defined as

$$\epsilon_i = \frac{\partial u_i}{\partial x_i} \quad \text{for } i = 1, 2, 3, \quad (3)$$

$$\epsilon_4 = \frac{\partial u_2}{\partial x_3} + \frac{\partial u_3}{\partial x_2}, \quad (4)$$

$$\epsilon_5 = \frac{\partial u_1}{\partial x_3} + \frac{\partial u_3}{\partial x_1}, \quad (5)$$

$$\epsilon_6 = \frac{\partial u_1}{\partial x_2} + \frac{\partial u_2}{\partial x_1}. \quad (6)$$

Note that the subscript of σ has changed from tensor notation in (1) to matrix notation in (2), as in Ref. [12], so that both the wave equation and Hooke's law may be expressed using the Einstein summation convention.

The computational effort required for the simulation is greatly reduced by assuming that the acoustic waves are of Rayleigh wave type, and therefore have no variation in the direction aligned parallel to the propagating wave front. Taking this direction to be along the x_2 -axis, all terms containing $\frac{\partial}{\partial x_2}$ may be set to zero. This reduces the number of independent terms on the RHS of (1) to two, or in the summation notation $j = 1, 3$, and in (2) the number of independent equations reduces from six to five as σ_2 is not used, so in the summation convention $i = 1, 3, 4, 5, 6$. The summations for the equations of motion and Hooke's law remain the same throughout the rest of this work so will no longer be shown. While the variation in the x_2 direction is assumed to be zero the displacement in this direction, u_2 , is not zero and therefore cannot be discounted. The problem may be simplified further if the solution is restricted to one particular crystal class such that many of the terms in (2) become zero due to symmetries within the crystal's unit cell. In the following derivation however, all terms within (2) have been included to make PMLs applicable to all crystal classes and therefore to be material independent.

Since the acoustic velocity inside a crystal is slow compared to the piezoelectric response, the induced charge displacement from the acoustic wave, ρ , is assumed to be adiabatic and takes the form

$$\rho = -\nabla_i \cdot e_{ij} \epsilon_j \quad \text{for } i = 1, 3; j = 1, 3, 4, 5, 6, \quad (7)$$

therefore allowing ϕ to be found by solving Poisson's equation

$$\nabla \cdot \epsilon \nabla \phi = -\rho. \quad (8)$$

In order to implement PML boundary conditions we split the second order time differential by introducing an auxiliary field, \mathbf{v} , such that (1) becomes

$$\rho \frac{\partial u_i}{\partial t} = \frac{\partial v_{ij}}{\partial x_j}, \quad (9)$$

where the time differential of \mathbf{v} is defined as

$$\frac{\partial v_i}{\partial t} = \sigma_i = C_{ij} \epsilon_j + e_{ik}^T \frac{\partial \phi}{\partial x_k}. \quad (10)$$

Transforming to the frequency domain, such that $\mathbf{u}(t) \rightarrow \mathbf{U}(\omega)$ and $\mathbf{v}(t) \rightarrow \mathbf{V}(\omega)$, we obtain

$$-i\omega \rho U_i = \frac{\partial V_{ij}}{\partial x_j}, \quad (11)$$

and

$$-i\omega V_i = C_{ij} \epsilon_j + e_{ik}^T \frac{\partial \phi}{\partial x_k}, \quad (12)$$

respectively, where ω is the angular frequency of the acoustic wave. We now introduce the complex change of variables such that $x_i \rightarrow (1 + i\frac{\zeta_i}{\omega})x_i$, where ζ has two components, $\zeta_1(x_1)$ and $\zeta_3(x_3)$, which are the absorption profiles of the PML in the x_1 and x_3 direction respectively, to give

$$-i\omega \rho U_i = \frac{1}{1 + i\frac{\zeta_j}{\omega}} \frac{\partial V_{ij}}{\partial x_j}, \quad (13)$$

and

$$\begin{aligned} -i\omega V_i = & C_{i1} \frac{1}{1 + i\frac{\zeta_1}{\omega}} \frac{\partial U_1}{\partial x_1} + C_{i3} \frac{1}{1 + i\frac{\zeta_3}{\omega}} \frac{\partial U_3}{\partial x_3} + C_{i4} \frac{1}{1 + i\frac{\zeta_3}{\omega}} \frac{\partial U_2}{\partial x_3} \\ & + C_{i5} \left(\frac{1}{1 + i\frac{\zeta_3}{\omega}} \frac{\partial U_1}{\partial x_3} + \frac{1}{1 + i\frac{\zeta_1}{\omega}} \frac{\partial U_3}{\partial x_1} \right) + C_{i6} \frac{1}{1 + i\frac{\zeta_1}{\omega}} \frac{\partial U_2}{\partial x_1} \\ & + e_{i1}^T \frac{1}{1 + i\frac{\zeta_1}{\omega}} \frac{\partial \phi}{\partial x_1} + e_{i3}^T \frac{1}{1 + i\frac{\zeta_3}{\omega}} \frac{\partial \phi}{\partial x_3}. \end{aligned} \quad (14)$$

Multiplying by $(1 + i\frac{\zeta_1}{\omega})(1 + i\frac{\zeta_3}{\omega})$ gives

$$-i\omega\rho U_i + \rho(\zeta_1 + \zeta_3)U_i + \frac{i}{\omega}\rho\zeta_1\zeta_3U_i = \frac{\partial V_{ij}}{\partial x_j} + \frac{i}{\omega} \left(\zeta_1 \frac{\partial V_{i3}}{\partial x_3} + \zeta_3 \frac{\partial V_{i1}}{\partial x_1} \right), \quad (15)$$

and

$$\begin{aligned} -i\omega V_i + (\zeta_1 + \zeta_3)V_i + \frac{i}{\omega}\zeta_1\zeta_3V_i &= C_{ij}\epsilon_j + e_{ik}^T \frac{\partial \phi}{\partial x_k} + \\ \frac{i}{\omega} \left(\zeta_1 \left\{ C_{i3} \frac{\partial U_3}{\partial x_3} + C_{i4} \frac{\partial U_2}{\partial x_3} + C_{i5} \frac{\partial U_1}{\partial x_3} + e_{i3}^T \frac{\partial \phi}{\partial x_3} \right\} \right. & \\ \left. + \zeta_3 \left\{ C_{i1} \frac{\partial U_1}{\partial x_1} + C_{i5} \frac{\partial U_3}{\partial x_1} + C_{i6} \frac{\partial U_2}{\partial x_1} + e_{i1}^T \frac{\partial \phi}{\partial x_1} \right\} \right). & \end{aligned} \quad (16)$$

Transforming back to the time domain gives

$$\rho \frac{\partial u_i}{\partial t} = \frac{\partial v_{ij}}{\partial x_j} - \rho(\zeta_1 + \zeta_3)u_i + \alpha_i, \quad (17)$$

where the auxiliary field α has been introduced in place of the $\frac{i}{\omega}$ terms in (15), which become time integrals when transformed to the time domain, such that the time derivative of α is

$$\frac{\partial \alpha_i}{\partial t} = \zeta_1 \frac{\partial v_{i3}}{\partial x_3} + \zeta_3 \frac{\partial v_{i1}}{\partial x_1} - \rho\zeta_1\zeta_3u_i, \quad (18)$$

and

$$\frac{\partial v_i}{\partial t} = C_{ij}\epsilon_j + e_{ik}^T \frac{\partial \phi}{\partial x_k} - (\zeta_1 + \zeta_3)v_i + \beta_i, \quad (19)$$

where the auxiliary field β has been introduced in place of the $\frac{i}{\omega}$ terms in (16), such that its time derivative is

$$\begin{aligned} \frac{\partial \beta_i}{\partial t} &= \zeta_1 \left\{ C_{i3} \frac{\partial u_3}{\partial x_3} + C_{i4} \frac{\partial u_2}{\partial x_3} + C_{i5} \frac{\partial u_1}{\partial x_3} + e_{i3}^T \frac{\partial \phi}{\partial x_3} \right\} \\ &+ \zeta_3 \left\{ C_{i1} \frac{\partial u_1}{\partial x_1} + C_{i5} \frac{\partial u_3}{\partial x_1} + C_{i6} \frac{\partial u_2}{\partial x_1} + e_{i1}^T \frac{\partial \phi}{\partial x_1} \right\} - \zeta_1\zeta_3v_i. \end{aligned} \quad (20)$$

As identified by Smith *et al.* [2], the most natural choice of discretisation grid for applying FDTD analysis to the acoustic wave equations of motion is an interlaced mesh, with grid points interlaced in both space and time, as depicted in Fig. 1. Here, u and ϕ are mapped to whole-integer values of x_1 , x_3 and t , while v is mapped to half-integer values. Applying the finite difference approximation, it then follows that a spatial derivative depends upon the field values at $\pm\frac{1}{2}$, which lie in between grid points. These *midpoints*

may be taken as the average of their adjacent points, i.e. for a spatial derivative in the direction x_1 at the point (i, k)

$$\frac{\partial v}{\partial x_1}(i, k) = \frac{\bar{v}(i + \frac{1}{2}, k) - \bar{v}(i - \frac{1}{2}, k)}{\delta x} \quad (21)$$

where \bar{v} represents the average of the neighbouring points, i.e.

$$\bar{v}(i + \frac{1}{2}, k) = \frac{v(i + \frac{1}{2}, k + \frac{1}{2}) + v(i + \frac{1}{2}, k - \frac{1}{2})}{2} \quad (22)$$

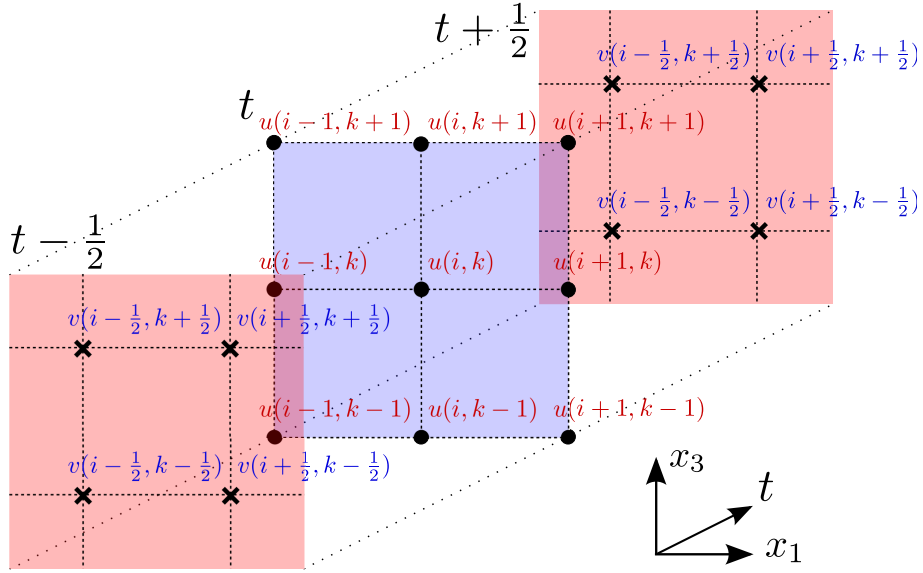


Figure 1: The interlaced mesh FDTD lattice shown for three half-integer time points.

As is normal with FDTD analysis, the instantaneous values of time-dependent variables are sampled midway between the time steps used in evaluating time-derivatives, such that (17) and (19) become

$$\rho \frac{u_i|_{t+1} - u_i|_t}{\delta t} = \left[\frac{\partial v_{ij}}{\partial x_j} - \rho(\zeta_1 + \zeta_3)u_i + \alpha_i \right]_{t+\frac{1}{2}}, \quad (23)$$

and

$$\frac{v_i|_{t+\frac{1}{2}} - v_i|_{t-\frac{1}{2}}}{\delta t} = \left[C_{ij}\epsilon_j + e_{ik}^T \frac{\partial \phi}{\partial x_k} - (\zeta_1 + \zeta_3)v_i + \beta_i \right]_t. \quad (24)$$

However, this implies a dependence on u and v at time steps between those to which these variables are mapped (i.e. $u_i|_{t+\frac{1}{2}}$ in (23) and $v_i|_t$ in (24)). This may be overcome

by first noting that these terms are zero within the region of interest and therefore any approximation that is made will not affect what we are trying to observe except possibly increase artificial reflections from the boundaries, and second realising that the difference between the spatial derivative at half time steps should be small provided that a small time step, δt is used. We therefore make the assumption that, in (23), $u_i|_{t+\frac{1}{2}} \approx u_i|_t$, and in (24), $v_i|_t \approx v_i|_{t-\frac{1}{2}}$ and note that doing so does not produce a noticeable increase in numerical noise from the PMLs in practice.

A similar problem arises when discretising the auxiliary fields α and β in time

$$\frac{\alpha_i|_{t+\frac{1}{2}} - \alpha_i|_{t-\frac{1}{2}}}{\delta t} = \left[\zeta_1 \frac{\partial v_{i3}}{\partial x_3} + \zeta_3 \frac{\partial v_{i3}}{\partial x_1} - \rho \zeta_1 \zeta_3 u_i \right]_t, \quad (25)$$

$$\begin{aligned} \frac{\beta_i|_t - \beta_i|_{t-1}}{\delta t} = & \left[\zeta_1 \left\{ C_{i3} \frac{\partial u_3}{\partial x_3} + C_{i4} \frac{\partial u_2}{\partial x_3} + C_{i5} \frac{\partial u_1}{\partial x_3} + e_{i3}^T \frac{\partial \phi}{\partial x_3} \right\} \right. \\ & \left. + \zeta_3 \left\{ C_{i1} \frac{\partial u_1}{\partial x_1} + C_{i5} \frac{\partial u_3}{\partial x_1} + C_{i6} \frac{\partial u_2}{\partial x_1} + e_{i1}^T \frac{\partial \phi}{\partial x_1} \right\} - \zeta_1 \zeta_3 v_i \right]_{t-\frac{1}{2}}. \end{aligned} \quad (26)$$

However, here the values of \mathbf{u} and \mathbf{v} at the half time step may be taken as the average of the adjacent time steps since they are already known, i.e.

$$u_i|_{t-\frac{1}{2}} = \frac{u_i|_t + u_i|_{t-1}}{2}, \quad (27)$$

and

$$v_{ij}|_t = \frac{v_{ij}|_{t+\frac{1}{2}} + v_{ij}|_{t-\frac{1}{2}}}{2}, \quad (28)$$

although we note, however, for simplicity, the same approximation as in (23) and (24) may be used and in practice the PMLs still have the desired effect.

The simulation domain for time-dependent variables is terminated by hard-wall boundaries so that the simulation takes the form shown in Fig. 2. For ϕ , Neumann boundary conditions are implemented. The hard-wall boundary condition is implemented on the whole-integer grid points, mapped to the variable \mathbf{u} , meaning that the outside edge of the PML, and therefore the maximum value of ζ , occurs at the half-integer grid points, mapped to \mathbf{v} , immediately inside of the hard-wall boundary.

The above derivation may easily be applied to the 3-dimensional acoustic wave equations of motion. However, in that case two $(\frac{1}{\omega})^2$ terms appear within the equations in the frequency domain, which become second-order time integrals in the time domain. These terms must then be dealt with by introducing two additional auxiliary fields.

$\zeta_x \neq 0$ $\zeta_z \neq 0$	$\zeta_z \neq 0$	$\zeta_x \neq 0$ $\zeta_z \neq 0$
$\zeta_x \neq 0$	Region of interest $\zeta_x = 0, \zeta_z = 0$	$\zeta_x \neq 0$
$\zeta_x \neq 0$ $\zeta_z \neq 0$	$\zeta_z \neq 0$	$\zeta_x \neq 0$ $\zeta_z \neq 0$

Figure 2: Illustration of the simulation domain showing the PMLs at the edges of the region of interest and where ζ is non-zero. Note that because ζ is zero within the region of interest the auxiliary fields α and β are also zero here.

3. Numerical results

We present an example of a bulk wave propagating radially outwards towards PML boundaries in the bismuth germanate ($\text{Bi}_4\text{Ge}_3\text{O}_{12}$) material system. Chagla *et al.* [3] previously showed that the use of boundary layers with quadratically-increasing damping coefficients led to instability in the simulated propagation of acoustic waves in this material. By way of comparison, we show that our proposed PML equations provide a stable and efficient means of absorbing incident waves.

The x_1 - and x_3 -axes of the simulation are aligned along the $[1,1,0]$ and $[0,0,1]$ crystal axes respectively by rotating the elastic and piezoelectric tensors by 45° about the $[0,0,1]$ crystal-axis such that an acoustic wave will propagate along the $[1,1,0]$ direction, as is done experimentally with cubic crystals. The excitation frequency used was 1 GHz, as in [3], making the spatial discretisation step, δx_1 and δx_3 , $0.15 \mu\text{m}$ (i.e., $\sim \frac{\lambda}{20}$). The grid size of the region of interest was set to 201×201 points and the time step, δt was set to 25 ps observing the FDTD stability criterion [13]. The PMLs used were 10-points thick ($\sim \frac{\lambda}{2}$) and the parameter ζ was increased quadratically up to its maximum stable value of $1.58 \times 10^{10} \text{ rad s}^{-1}$ as described in the following section.

The acoustic wave was excited by setting a 3×3 square in the centre of the simulation domain to have a constant charge which was then oscillated sinusoidally at the excitation

frequency for two periods and solving Poisson’s equation to find the potential profile around this charge over the simulation domain. This potential profile was used as an input to the acoustic wave equations of motion to launch a propagating wave. This method of excitation was used firstly because it is more physically realistic than exciting a component of the displacement since acoustic waves in piezoelectric crystals are generated using an alternating potential, and secondly because excitations at a single point tend to lead to instabilities caused by the change in sign of the spatial differential from the point of excitation to its surrounding points. These instabilities manifest themselves as changes in the sign of the solution from one grid point to the next such that the entire solution appears modulated by a sawtooth wave with oscillations of the order of the grid spacing. Fig. 3 shows the resulting acoustic wave propagating in bulk bismuth germanate, with material parameters taken from [14], which is absorbed by the PML boundaries.

4. Stability and optimisation of the PML

The discretized PML equations will be subject to a system-dependent stability criterion, much the same as the stability criterion for the unmodified equations within the region of interest. Considering the stability criterion for FDTD analysis in two dimensions [13]

$$v_{\max}\delta t = \left(\frac{1}{\delta x_1^2} + \frac{1}{\delta x_2^2} \right)^{-\frac{1}{2}}, \quad (29)$$

where δt , δx_1 and δx_3 are the discretisation parameters in time and space respectively and v_{\max} is the maximum velocity within the simulation domain, it is clear that within the PML layers extra terms will be added to this criterion which have a dependence upon ζ (or more accurately a dependence upon the maximum value of ζ within the PML since this represents the *worst case* scenario). It is important for the maximum stable value of ζ to be found since the attenuation of a propagating wave within PML regions is proportional to the value of ζ . Therefore, the effectiveness of the PMLs will be increased if a larger stable value of ζ is used. From (29), it may be inferred that the maximum stable value of ζ will have a dependence upon the discretisation parameters, δt , δx_1 and δx_3 , as well as the material system being examined since $v_{\max} = \sqrt{C/\rho}$ where C is the elastic constant in the direction of maximum velocity. Surprisingly however, the

maximum stable value of ζ also has a dependence upon the thickness of the PML as well as how ζ varies through the PML. Although the derivation of universal stability limits of ζ is challenging, insight may be gained into the effect of PML thickness and functional forms of ζ by examining the stability limits numerically for a given system.

In order to systematically examine the maximum stable value of ζ we restrict its functional form to

$$\zeta_i(x_i) = \zeta_{\max} \left(\frac{|x_i - x_{i,\text{PML}}|}{\Delta_{\text{PML}}} \right)^a \quad (30)$$

where ζ_{\max} is the maximum value of ζ inside the PML, x_i is the position in the x_1 and x_3 directions, $x_{i,\text{PML}}$ is the position of the boundary between the ROI and the PML and Δ_{PML} is the thickness of the PML. The shape of the ζ function may then be controlled using the parameter a , such that $a = 1$ gives a linear increase from zero at the inside edge of the PML up to ζ_{\max} at the outside edge, $a = 2$ a quadratic increase and so on. The case for $a = 0$ has been omitted since, once discretised, the PMLs cease to be perfectly matched and therefore a sudden step in ζ produces sizeable reflections from the interface between the ROI and PML which were found to be around two orders of magnitude larger than the reflected waves with steadily increasing ζ values. The maximum stable value of ζ_{\max} (with a given shape and PML thickness) was then found by using a bisection search where the simulation was deemed to be unstable if after simulating 25 ns, by which time the initial excitation would have been absorbed by the PML, the oscillations within the simulation domain are larger than the initial excited acoustic pulse. Because instabilities within the simulation domain grow exponentially this method finds the stability limit for ζ_{\max} in the chosen system reliably. Figure 4 shows the maximum stable values of ζ_{\max} found for a range of values of Δ_{PML} and a for the bismuth germanate material system examined in the preceding section.

To compare the effectiveness of the PMLs with different values of a , the amplitude of the wave reflected back from the boundaries was measured. This was done by performing a Fourier decomposition on the u_3 component of displacement at a point next to one of the PML boundaries over time in order to separate the reflected signal at the excitation frequency of 1 GHz from the higher frequency transients, which exist behind the excited pulse and come from the excitation being switched off suddenly after two periods. The point used was central on the x_3 -axis and 40 points ($6 \mu\text{m}$) from the inside edge of one of

the PML boundaries perpendicular to the x_1 -axis to allow the two periods of the excited wave to pass through the point before the reflected wave arrives back at the same point. The top inset in Fig. 4 shows maximum amplitudes of the reflected waves normalised to the maximum amplitude of the excited wave for different values of a and Δ_{PML} . The maximum stable value of ζ_{max} was used in each case. For PMLs below 10-points thick, ζ with $a = 2$ is the most effective although for higher numbers of points, particularly above 20 points, all PMLs give similar performance.

Although the numerical analysis above provides a method of optimizing PML parameters for a given system, this may not be feasible for larger simulation domains, in which much longer run times would be required. Ideally, the PML parameters could be found *ab initio* for any system by applying a universal stability criterion. However, the derivation of such a criterion is challenging, and as an interim measure a more conservative choice of ζ_{max} (i.e., much lower than those found for the example above) is likely to yield stable simulations in a wider range of simulation domains. As such, we have also examined the stability of the system considered above (using a range of shape parameters, a) when ζ_{max} has been restricted to the much lower constant value of $1 \times 10^{10} \text{ rad s}^{-1}$. This value of ζ_{max} is equal to $\frac{1}{4\delta t}$ and since ζ_{max} is roughly inversely proportional to δt , this represents a sensible choice for a stable value of ζ_{max} that is dependant upon the simulation parameters and the material system (as δt is material dependent). The bottom inset of Fig. 4 shows the amplitude of the reflected wave for different values of a and Δ_{PML} . Here we clearly see that $a = 1$ has the best performance for PMLs thinner than around 20 points. This is because higher values of a give rise to smaller ζ close to the ROI, and therefore the net attenuation of the wave within the PML is reduced.

If a similar stability analysis was applied to a 3-dimensional system, then a similar trend for the stability of the PML would be expected with regards to its operating parameters. However, since the stability criterion for 3-dimensional systems stipulates that δt will be smaller if the three spatial steps are equal to the two in a 2-dimensional system, and since ζ_{max} should still be inversely proportional to δt , it is expected that higher values of ζ_{max} may be used.

5. Conclusion

PML boundary conditions have been derived for FDTD analysis of acoustic waves within piezoelectric crystals. The robustness and effectiveness of these boundary conditions has been demonstrated in simulations of wave propagation in bismuth germanate—a system in which simple absorbing boundary conditions have been previously shown to cause instabilities. A numerical investigation into the stability of the discretised PML equations with respect to the PML parameter ζ has been presented for the aforementioned material system, showing a dependence on both how this parameter varies within the PML and the thickness of the PML. The effectiveness of the PML has been analyzed in terms of the reduction in amplitude of the reflected wave from the boundary of the simulation domain in the bismuth germanate system. It was found that any spatially-varying PML parameter ζ yields the same PML effectiveness, provided that ζ increases monotonically from zero at the edge of the ROI up to a maximum stable value, ζ_{\max} , at the edge of the simulation domain. It would, therefore, be desirable to determine a universally applicable analytical form of ζ_{\max} such that the PML effectiveness of any system may be optimized *ab initio*. However, the exact form of the stability criterion for the discretized PML equations may be challenging to find, and at present ζ_{\max} must be found numerically for a given system. Since this numerical optimization may be impractically time consuming for large simulation domains, stable (but less effective) PMLs may be realised by limiting ζ to a lower-than-optimal value, which may be estimated from simulations of simpler systems. In this suboptimal case, we have shown that the PML effectiveness is highest if a low-order (e.g., linear) spatial variation in ζ is used. Similar trends for the performance of the PMLs can be expected in other material systems, although further theoretical analysis of the stability criterion will be required for confirmation. Nevertheless, the presented boundary conditions will allow for accurate and robust simulation of open-domain acoustic wave problems in piezoelectric crystals.

References

- [1] K. Yee, Numerical solution of initial boundary value problems involving Maxwell's equations in isotropic media, *Antennas and Propagation, IEEE Transactions on* 14 (3) (1966) 302–307. doi:10.1109/TAP.1966.1138693.

- [2] P. M. Smith, R. Ren, Finite-difference time-domain techniques for SAW device analysis, in: *Ultrasonics Symposium*, 2002. Proceedings. 2002 IEEE, Vol. 1, 2002, pp. 325–328. doi:10.1109/ULTSYM.2002.1193341.
- [3] F. Chagla, P. M. Smith, Finite difference time domain methods for piezoelectric crystals, *Ultrasonics, Ferroelectrics and Frequency Control*, IEEE Transactions on 53 (10) (2006) 1895–1901. doi:10.1109/TUFFC.2006.122.
- [4] J. Berenger, A perfectly matched layer for the absorption of electromagnetic waves, *Journal of Computational Physics* 114 (2) (1994) 185–200. doi:10.1006/jcph.1994.1159.
URL <http://www.sciencedirect.com/science/article/pii/S0021999184711594>
- [5] F. L. Teixeira, W. C. Chew, General closed-form PML constitutive tensors to match arbitrary bianisotropic and dispersive linear media, *IEEE Microwave and Guided Wave Letters* 8 (6) (1998) 223–225. doi:10.1109/75.678571.
- [6] F. L. Teixeira, W. C. Chew, Complex space approach to perfectly matched layers: a review and some new developments, *International Journal of Numerical Modelling-Electronic Networks Devices and Fields* 13 (5) (2000) 441–455. doi:10.1002/1099-1204(200009/10)13:5<441::AID-JNM376>3.0.CO;2-J.
- [7] A. F. Oskooi, L. Zhang, Y. Avniel, S. G. Johnson, The failure of perfectly matched layers, and towards their redemption by adiabatic absorbers, *Optics Express* 16 (15) (2008) 11376–11392. doi:10.1364/OE.16.011376.
- [8] W. Shin, S. Fan, Choice of the perfectly matched layer boundary condition for frequency-domain Maxwell's equations solvers, *Journal of Computational Physics* 231 (8) (2012) 3406–3431. doi:10.1016/j.jcp.2012.01.013.
URL <http://www.sciencedirect.com/science/article/pii/S0021999112000344>
- [9] N. Feng, J. Li, Novel and efficient FDTD implementation of higher-order perfectly matched layer based on ADE method, *Journal of Computational Physics* 232 (1) (2013) 318–326. doi:10.1016/j.jcp.2012.08.012.
URL <http://www.sciencedirect.com/science/article/pii/S0021999112004585>
- [10] W. C. Chew, Q. H. Liu, Perfectly matched layers for elastodynamics: A new absorbing boundary condition, *Journal of Computational Acoustics* 4 (4) (1996) 341–359. doi:10.1142/S0218396X96000118.
- [11] F. Q. Hu, A stable, perfectly matched layer for linearized Euler equations in unsplit physical variables, *Journal of Computational Physics* 173 (2) (2001) 455–480. doi:10.1006/jcph.2001.6887.
URL <http://www.sciencedirect.com/science/article/pii/S0021999101968871>
- [12] J. F. Nye, R. B. Lindsay, *Physical Properties of Crystals: Their Representation by Tensors and Matrices*, Clarendon Press, Oxford, 1957.
- [13] A. Taflov, M. E. Brodwin, Numerical solution of steady-state electromagnetic scattering problems using the time-dependent Maxwell's equations, *Microwave Theory and Techniques*, IEEE Transactions on 23 (8) (1975) 623–630. doi:10.1109/TMTT.1975.1128640.
- [14] H. Schwerpe, Electromechanical properties of bismuth germanate $\text{Bi}_4(\text{GeO}_4)_3$, *Sonics and Ultra-*

sonics, IEEE Transactions on 16 (4) (1969) 219. doi:10.1109/T-SU.1969.29531.

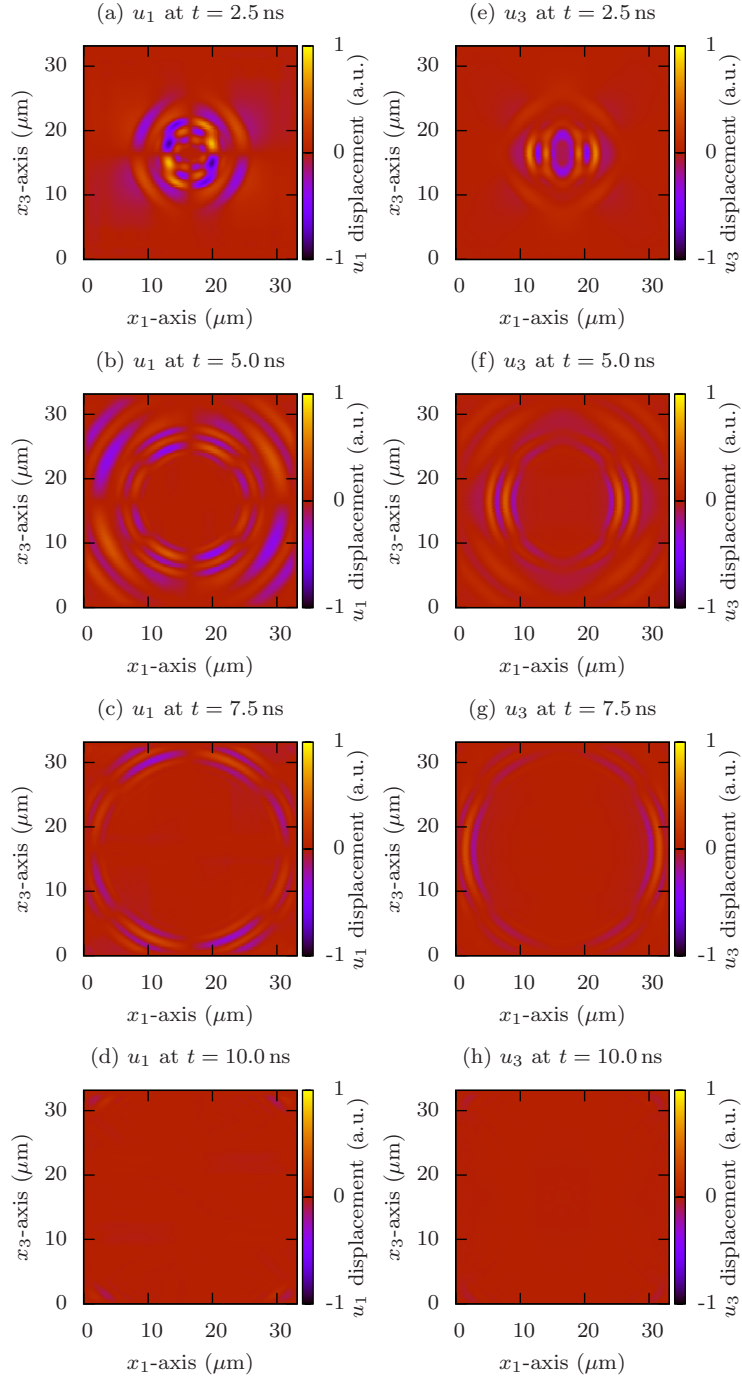


Figure 3: The u_1 and u_3 displacement components for the acoustic wave launched in $\text{Bi}_4\text{Ge}_3\text{O}_{12}$ showing how the wave propagates radially outwards and is absorbed by the PML. (Animations of the propagating wave are included as supplementary material. Animation 1 for the u_1 displacement and animation 2 for the u_3 displacement.)

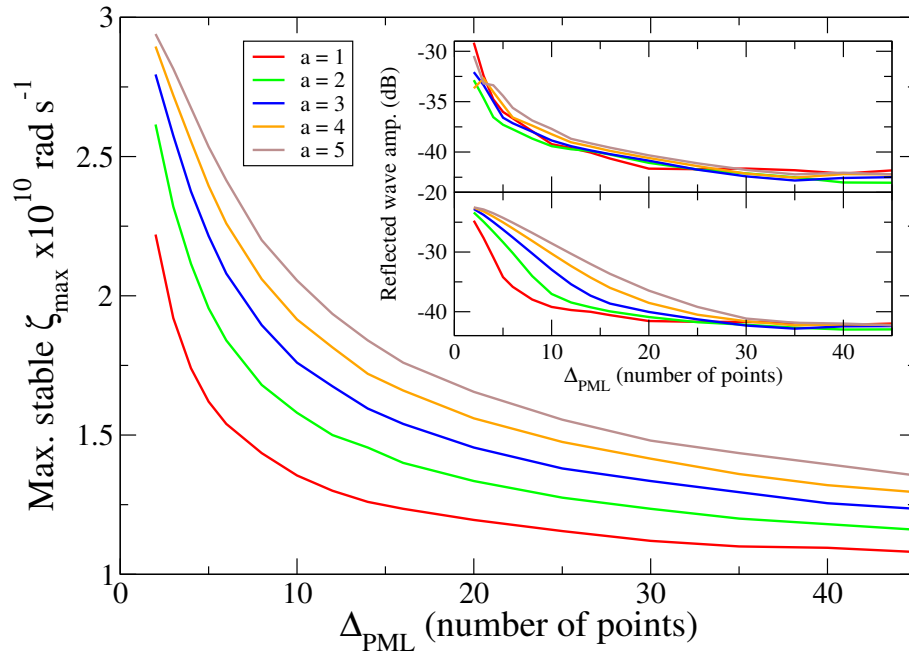


Figure 4: Variation in the maximum stable value of ζ_{\max} with Δ_{PML} from 2 to 45 points ($\lambda = 20$ points) and with the ζ shape factor a . (*Top inset*) The maximum amplitude of reflection from PML with varying a and Δ_{PML} using the maximum stable value of ζ_{\max} for each case, normalised to the maximum amplitude of the excited wave. (*Bottom inset*) The maximum amplitude of reflection from PML with varying a and Δ_{PML} using a constant value of $\zeta_{\max} = 1 \times 10^{10} \text{ rad s}^{-1}$.